Reversible conformational change coupled electron transfer (CCET) for stable redox-active molecules

Christian Malapit

christian.malapit@northwestern.edu

Northwestern University https://orcid.org/0000-0002-8471-4208

An Kitamura

Northwestern University

Jake Evans

Northwestern University

Article

Keywords:

Posted Date: June 12th, 2025

DOI: https://doi.org/10.21203/rs.3.rs-6835054/v1

Additional Declarations: There is **NO** Competing Interest.

Reversible conformational change coupled electron transfer (CCET) for stable redox-active molecules

An Kitamura, Jake M. Evans, Christian A. Malapit*

Department of Chemistry, Northwestern University, Technological Institute, Evanston, Illinois 60208, United States

*Correspondence to: christian.malapit@northwestern.edu

Abstract

Reversible electron transfer is a fundamental process that is essential in redox-active organic molecules and materials (ROMs) across biological, chemical, and energy technologies. Achieving stable and reversible redox behavior often requires careful molecular design or coupling electron transfer with a chemical step, such as proton-coupled electron transfer (PCET). In this study, we investigate a distinct stabilization mechanism based on *conformational change coupled electron transfer* (CCET). We show that acyclic 1,2-dicarbonyl compounds exhibit enhanced electrochemical stability by undergoing a conformational shift from skewed *cis*-geometries to more stable *trans*-conformations upon reduction, enabling stability even at more negative reduction potentials. Mechanistic studies demonstrate that CCET stabilizes the reduced state by allowing bond rotation that minimizes electron repulsion and delocalizes electron density by retaining a *trans*-planar geometry. Unlike PCET, which shifts reduction potentials positively, CCET enhances stability even at more negative potentials—breaking the conventional trade-off between redox potential and stability. Charge-discharge cycling of benzil shows 99.8% capacity retention over 500 cycles, demonstrating CCET as a powerful strategy for developing stable, high-performance ROMs for potential energy storage applications.

Introduction

The development of redox-active organic molecules (ROM) has seen extensive advancement, especially in fields of energy storage, electrocatalysis, and photoredox systems.[1–9] In these applications, a chemically reversible electron transfer (ET) is essential and are often achieved by molecular design, such as extended conjugation, or by coupling ET with a chemical step, as in proton-coupled electron transfer (PCET, Fig. 1a).[10-18] While both strategies are well utilized in many important technologies, they often present a trade-off between stability and redox potential—two key parameters in energy and catalytic systems. As such, we seek to find molecular frameworks capable of reversible ET coupled with mechanistically distinct, stability-inducing structural changes. Inspired by the well-studied reversible azobenzene photoisomerization,[19–22] and electrochemically induced *cis*-*trans* isomerization in coordination complexes (albeit irreversible) (Fig. 1b),[23] we hypothesized that structurally flexible frameworks could achieve stability through electrochemically induced geometrical transformations.

Most stable ROMs feature rigid, conjugated backbones that offer stability through resonance or conjugation and do not present conformational flexibility.[9,24] For example, anthraquinone (AQ), a cyclic 1,4-dicarbonyl compound, is one of the most widely studied ROM due to its exceptional stability through conjugation and PCET in aqueous systems (Fig. 1a).[25–27] Interestingly, phenanthrenequinone (PQ), a cyclic 1,2-dicarbonyl compound, also undergoes reversible ET but showed poor long-term cycling stability.[28,29] We hypothesized that the formation of a *trans*-radical anion in 1,2-dicarbonyl compounds may minimize electrostatic repulsion and further enhance electrochemical stability, however, this is impossible with cyclic systems due to the lack of geometric flexibility around the dicarbonyl C–C bonds. Guided by this idea, we identified flexible, acyclic 1,2-dicarbonyl compounds as frameworks for a reversible ET accompanied by conformational change.[30–37] Indeed, benzil (Bz), an acyclic 1,2-dicarbonyl, has previously been used as structural units in macromolecular and polymeric solid electroactive materials for metal-ion batteries or pseudo capacitors owing to its electrochemical properties.[38–42]

Here, we investigate the underlying mechanism of conformational change coupled electron transfer (CCET) in various acyclic 1,2-dicarbonyl compounds, and compare them to their rigid, cyclic analogs. These mechanistic insights enabled the development of simple, highly stable and soluble ROMs with highly negative redox potentials. More importantly, in contrast to PCET and molecular stabilization by electronics and conjugation, CCET in 1,2-dicarbonyl compounds overcomes the traditional trade-off between redox potential and stability.

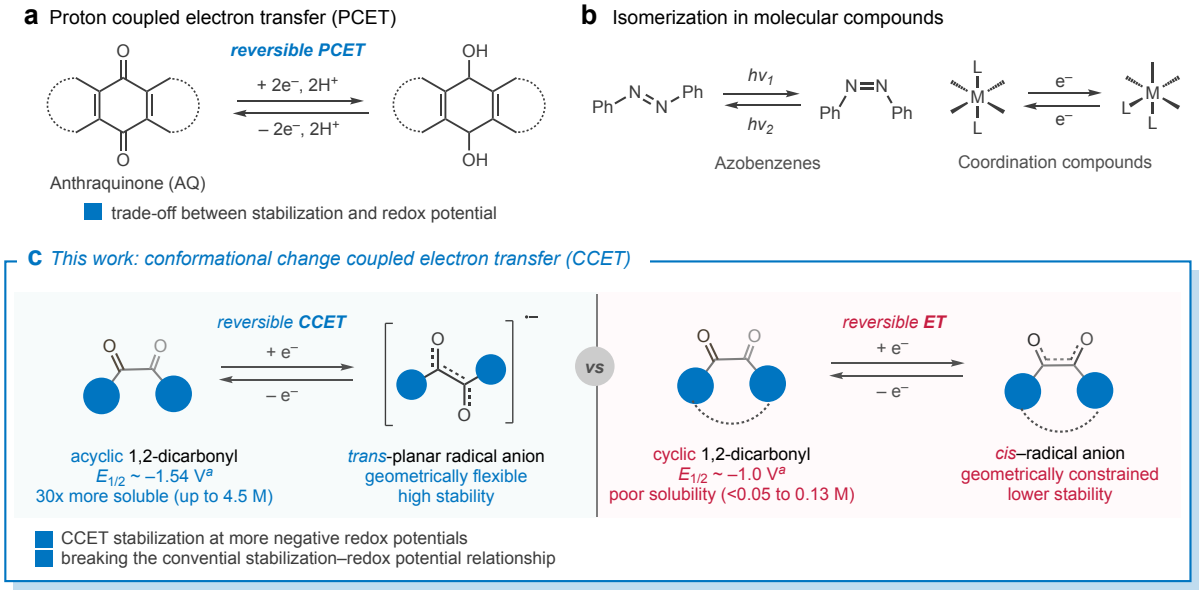

Figure 1. Coupled electron transfer reactions and isomerization. (a) Proton-coupled electron transfer (PCET) in anthraquinone (AQ). (b) Examples of geometrical *cis-trans* isomerization in azobenzene and of coordination complexes (c) This work, conformational change coupled electron transfer (CCET) using acyclic 1,2-dicarbonyls compounds compared to geometrically constrained electron transfer.

Results and Discussion

We began our investigation by characterizing PQ and Bz using cyclic voltammetry (CV) in 0.5 M $TBAPF_6$/DMF (Fig. 2a). Redox potentials and reversibility were compared between cyclic (PQ) and acyclic (Bz) 1,2-dicarbonyl structures. PQ displayed a redox potential of –1.0 V vs. Fc/Fc^+, while Bz exhibited a more negative potential of –1.54 V vs. Fc/Fc^+, consistent with the expectation that the less conjugated Bz is harder to reduce. Despite this, both compounds showed high electrochemical reversibility, with cathodic-to-anodic peak current ratios (i_{pa}/i_{pc}) above 0.95 (Table S1). Notably, Bz exhibits reversible reduction at a lower potential without extended conjugation, suggesting an alternative stabilization mechanism. The Randles-Sevcik analysis derived from scan-rate dependent CVs display linear and symmetric plots, indicating a reversible, diffusion-controlled single-electron transfer process (Fig. 2a). These results imply that stabilization mechanism is intrinsically coupled to the electron transfer step, yet and not directly observable under standard CV conditions. Other acyclic structures had redox potentials more negative than the corresponding cyclic analogs as can be seen in 2,2'-thenil and 3,3'-thenil. Furil, an acyclic 1,2-dicarbonyl structure with furans had a redox potential of –1.40 V. Moreover, the diffusion coefficients of all tested compounds had values comparable to ROMs commonly used as anolytes in redox flow batteries (RFBs) (Table S1).

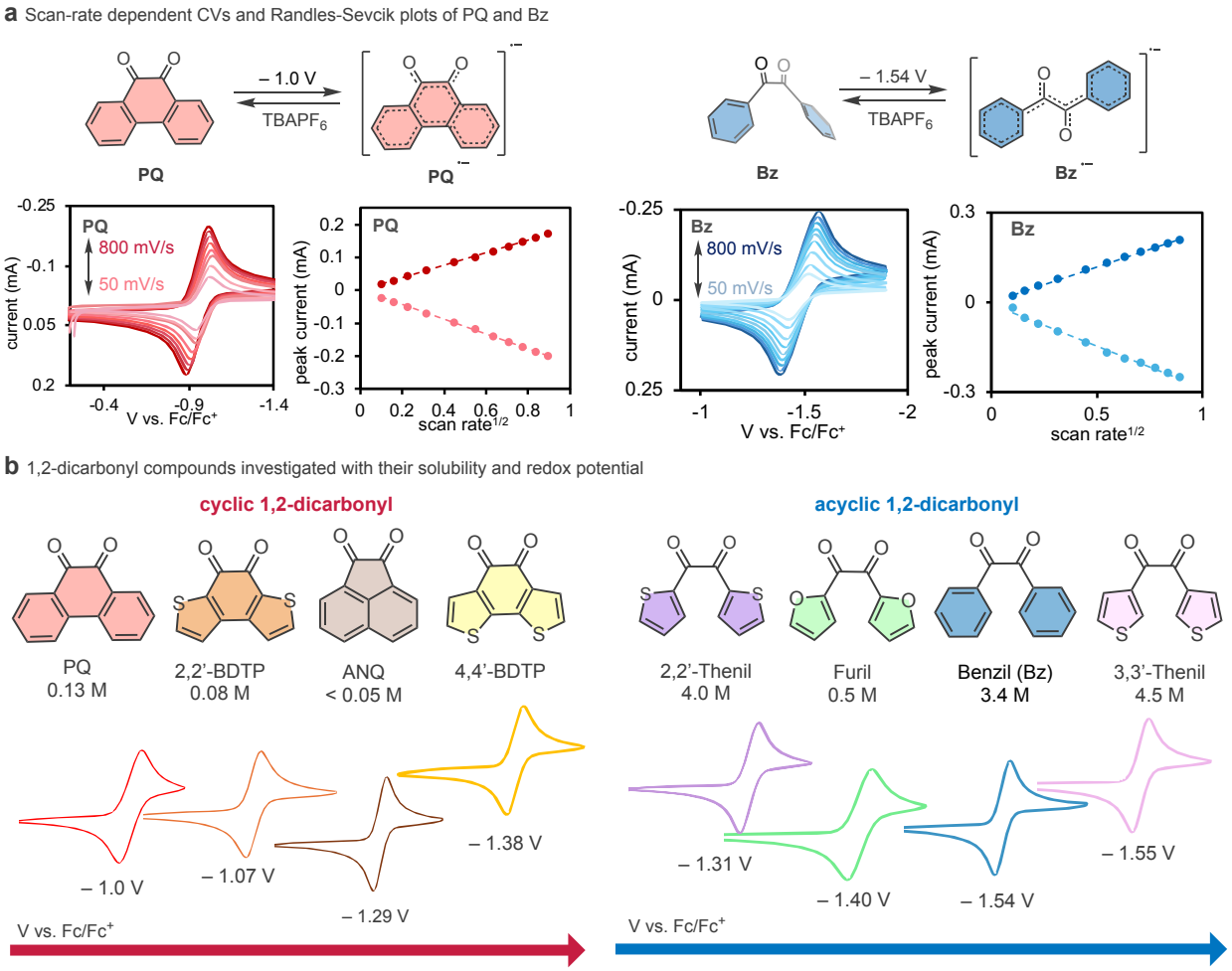

Figure 2. Electrochemical properties of various cyclic and acyclic 1,2-dicarbonyl compunds. (a) Single electron reduction schemes and CVs of 5 mM PQ and Bz scanned at scan rates from 50 to 800 mV/s referenced against ferrocene. Randles-Sevcik plots of peak current vs. square root of scan rate. (b) Structures, solubilities, redox potentials V vs. Fc/Fc^+, and cyclic voltammograms (CV) in 0.5 M TBAPF6 DMF of 5 mM phenanthrenequinone (PQ), benzo[1,2-b:4,3-b']dithiophene-4,5-dione (2,2'-BDTP), acenaphthenequinone (ANQ), benzo[2,1-b:3,4-b']dithiophene-4,5-dione (4,4'-BDTP), 2,2'-thenil, furil, benzil, and 3,3'-thenil.

Using benzil as a model compound, we performed various spectroscopic techniques to determine the conformation of the electrochemically generated reduced species and observe CCET. Bz was reduced with constant current bulk electrolysis in 0.5 M $TBAPF_6$/DMF that generated a dark blue solution (Fig. 3a). A single radical species was detected with electron paramagnetic resonance (EPR) spectroscopy (Fig. 3a). Simulations of the hyperfine splitting constants for the phenyl ring hydrogens ortho, meta, and para to a carbonyl are equivalent to those on the other ring (Fig. S38). This suggests the unpaired electron is delocalized throughout the structure, indicating greater planarity from the initially skewed structure.

Fourier-transform infrared (FT-IR) and Raman spectroscopy studies of Bz provide substantial information into its molecular geometry. Several literature sources have examined this topic, supporting a *cis*-skewed geometry in the neutral state and a *trans*-planar geometry in the triplet state.[30,33,43–48] Here, FT-IR and Raman data were collected for neutral Bz and the electrochemically generated radical anion to determine whether the *trans*-planar geometry is conserved under our conditions. The FT-IR spectrum of neutral Bz aligns well with literature values (Table S3), with the C=O stretching vibrations serving as key indicators of conformation. Upon reduction, we observed a significant downshift in the C=O stretching band from 1670 cm^{-1} to 1390 cm^{-1} which is consistent with previously reported triplet-state or radical-anion forms.[43,48,49] This shift suggests increased delocalization and planarity in the reduced species. The radical anion also exhibits primarily sharp singlet absorption bands as may be expected of an increase in symmetry. Group

theory analysis supports this conclusion, as two C=O stretching modes (A, B) would be expected to be IR-active in the case of neutral Bz with C_2 symmetry while only one is IR-active in the case of a *trans*-planar molecule with C_{2h} symmetry (B_u) (Table S7). Thus, the presence of both an antisymmetric and symmetric C=O stretch in the neutral FT-IR spectrum and only one antisymmetric C=O stretch in the radical anion supports the hypothesis that the Bz adopts a *trans*-planar geometry upon reduction.

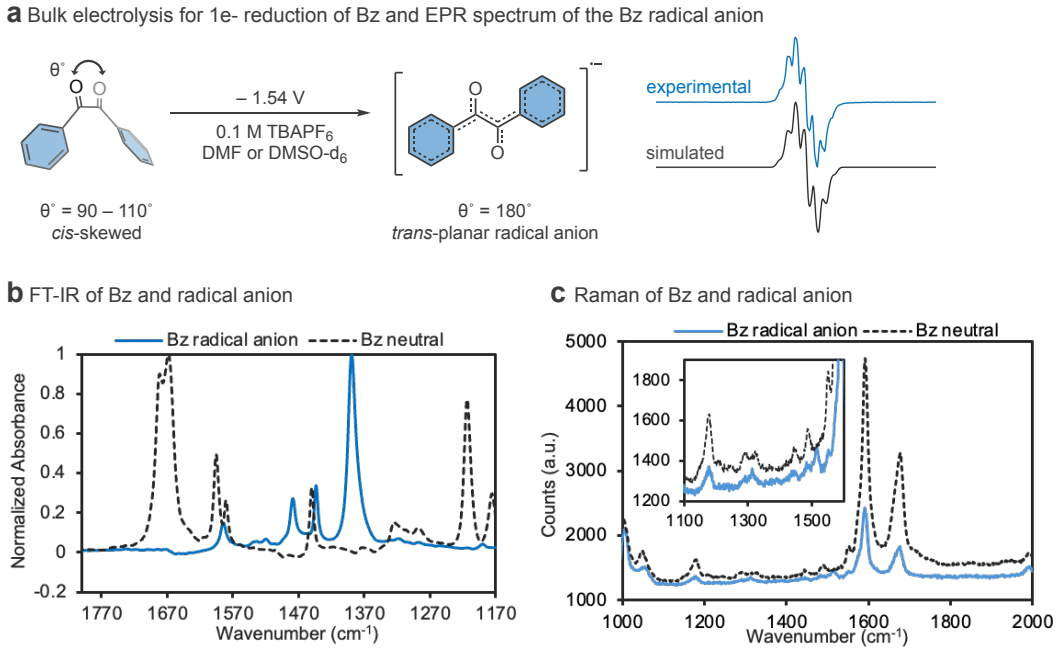

Figure 3. (a) Bulk electrolysis for the generation of electrochemically reduced Bz radical anion and EPR spectrum (blue) and simulated spectrum (black). (b) FT-IR spectrum of 20 mM Bz neutral (black) and radical anion (blue) in 0.1 M $TBAPF_6$, DMSO-d_6. (c) Raman spectrum of 20 mM Bz neutral (black) and radical anion (blue) in 0.1 M $TBAPF_6$, DMSO-d_6.

Raman spectrum collected for neutral Bz shows two C=O bands at 1591 and 1673 cm^{-1}, corresponding to symmetric and antisymmetric stretches, respectively, in agreement with literature, supporting the conclusion that neutral Bz is *cis*-skewed in the electrolyte used (Fig. 3c, Table S5).[44,46,46,49] In contrast, the *trans*-planar C_2h radical anion is expected to display only the symmetric A_g mode. Consistent with this, the radical anion spectrum shows a decrease in *cis*-associated bands and the appearance of a weak band at 1517 cm^{-1} (Fig. 3c, Table S6). Upon brief exposure to air, the 1517 cm^{-1} band disappears and the *cis*-associated features re-emerge (Fig. S46), confirming reversible interconversion between *trans* and *cis* forms.[44,50–52] Taken together, EPR, FT-IR, and Raman data confirm the formation of a *trans*-planar Bz radical anion upon reduction. These spectroscopic observations validate a conformation change electron transfer (CCET) mechanism, wherein Bz undergoes a geometric transformation from *cis*-skewed to *trans*-planar, enhancing planarity and electron delocalization in the reduced state.

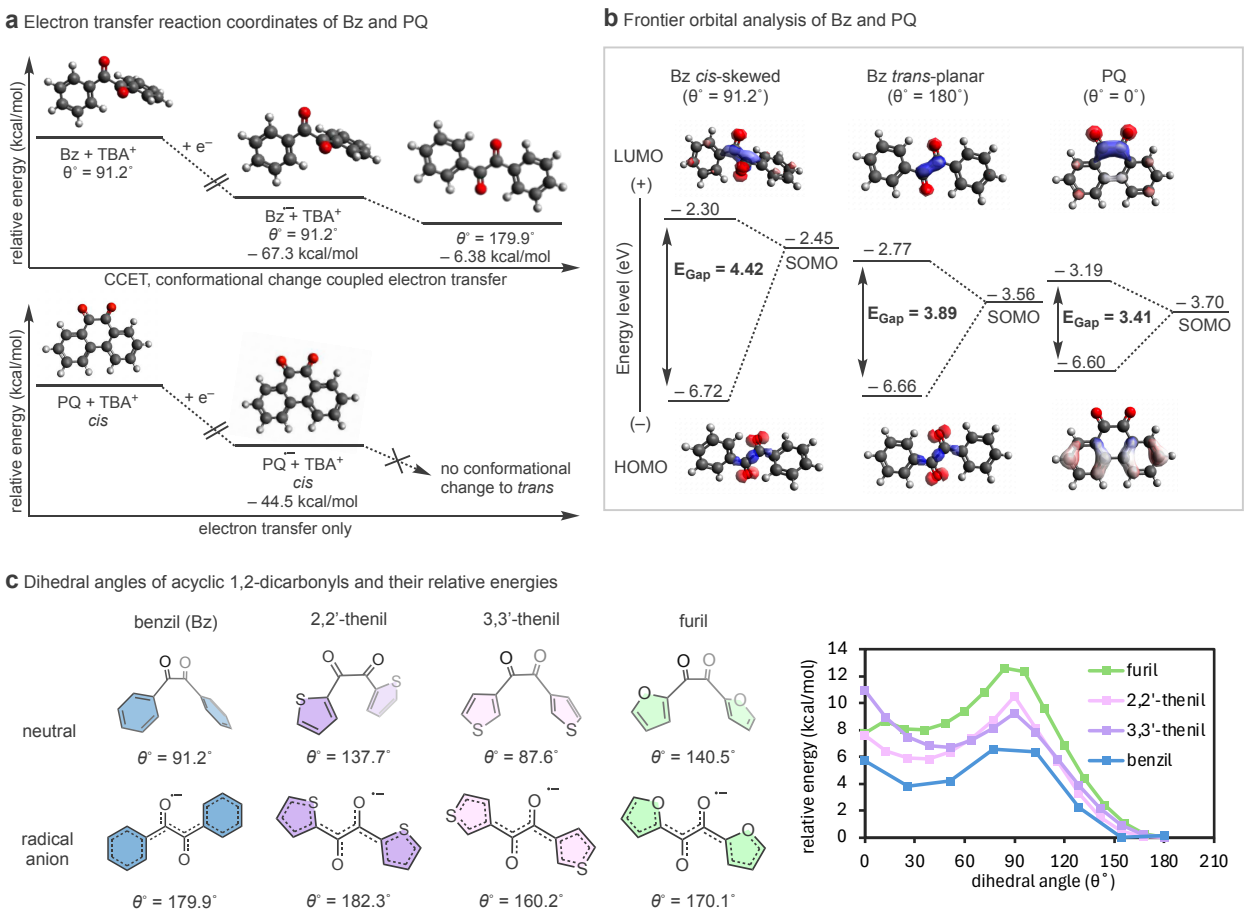

Figure 4. Computational studies. (a). DFT calculated energy diagram with optimized geometries for the one-electron reduction of Bz and PQ and their corresponding dicarbonyl dihedral angles, θ°. (b) Frontier orbitals of Bz with *cis*-skewed and *trans*-planar geometries and of PQ. (c) Computationally optimized dihedral angles of neutral and radical anions and their relative energies.

DFT calculations were conducted to evaluate how CCET influences radical anion stability and redox potentials. The neutral geometry of benzil (Bz) adopts a *cis*-skewed conformation with a dicarbonyl dihedral angle (θ°) of 91.2°, consistent with crystallographic data.[35] Upon reduction, the radical anion relaxes to a *trans*-planar geometry (θ° = 179.9°), in agreement with spectroscopic analysis (Fig. 4a). Energy scans across dihedral angles show that the *cis*-skewed radical anion is 6.38 kcal/mol higher in energy than the *trans*-planar form (Fig. 4c), indicating that bond rotation upon reduction is strongly favored. In contrast, no such conformational change is observed for the rigid cyclic phenanthrenequinone (PQ). Mulliken charge analyses show that the negative charge in both Bz and PQ radical anions is predominantly localized on the carbonyl oxygens (72% for Bz, 70% for PQ), with the unpaired electron also delocalized across the dicarbonyl system (Figs. S64, S68). This results in a highly electron-dense region in the *cis*-conformation, suggesting that intramolecular repulsion contributes to its instability. Thus, CCET enables rotation to a *trans*-conformation that minimizes electron repulsion at redox-active sites.

Repulsion and degree of conjugation was found to influence the redox system based on frontier orbital analysis (Fig. 4b). PQ, with extended conjugation, has a lower LUMO than Bz, consistent with its more positive redox potential (Fig. 4b). Additionally, the LUMO of *cis*-Bz is higher than that of *trans*-Bz, indicating that the skewed geometry hinders reduction. The SOMO energy of *cis*-Bz radical anion is 1.25 eV higher than PQ, while *trans*-Bz is only 0.14 eV higher, emphasizing the stabilizing effect of conformational reorganization even at more negative reduction potentials. Optimized geometries of other acyclic 1,2-dicarbonyls show a consistent trend: neutral species favor cis-skewed conformations, while their radical anions stabilize in trans-planar geometries (Figs. 4c, S47). Energy scans confirm that, like Bz, all

tested compounds exhibit increasing instability as the dihedral angle approaches *cis* (Fig. 4c S48–S50), further supporting CCET as a general stabilization mechanism.

High solubility is critical to prevent passivation of electrodes in redox catalysis and to maximize energy density in redox flow batteries (RFBs). Notably, acyclic 1,2-dicarbonyl structures had solubilities ranging from 0.5 to 4.5 M in DMF and are over thirty times greater than their cyclic counter parts (<0.05 to 0.13 M). Highly conjugated and planar organic structures often suffer from low solubility in polar organic solvents.[53,54] The reduced symmetry and structural flexibility in the acyclic structures could contribute to enhanced solubility.

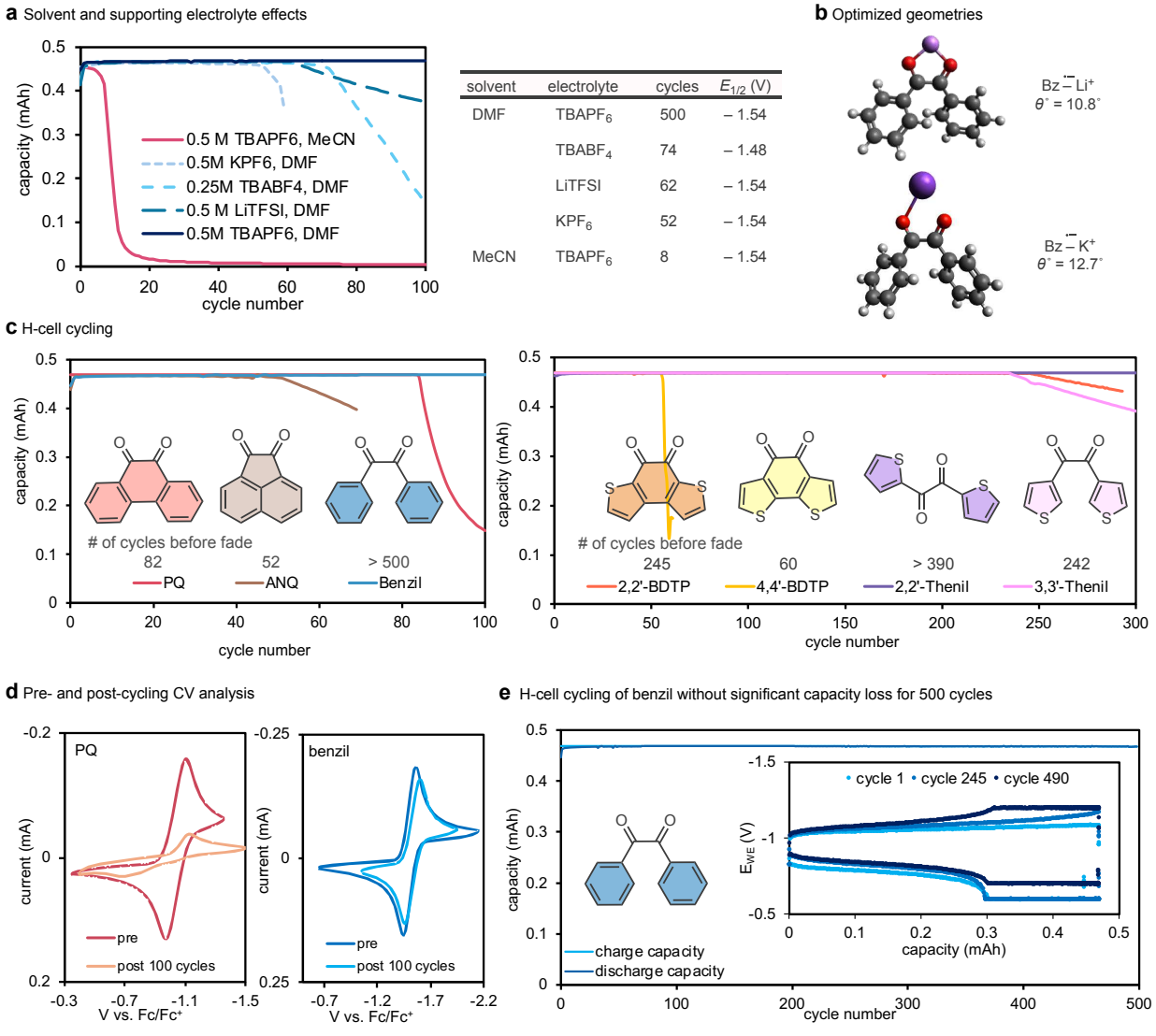

Figure 5. Static H-cell charge-discharge cycling studies of various 1,2-dicarbonyl compunds. (a) Static asymmetric H-cell cycling of 5 mM Bz in DMF and MeCN with different supporting electrolytes, number of cycles with 99% capacity retention, redox potentials (V vs. Fc/Fc^+). (b) Optimized geometries of Bz radical anion coordinated with Li^+ and K^+ counterion. (c) Static asymmetric H-cell cycling in 0.5 M TBAPF6, DMF with 1.1 equivalent ferrocene catholyte in the counter side, 5 mM ANQ, PQ, and Bz in the working side (left) and 5 mM 2,2'-BDTP, 4,4'-BDTP, 2,2'-thenil, and 3,3'-thenil in the working side (right). (d) CVs of Bz and PQ taken before and after 100 cycles. (e) Extended H-cell cycling with 5 mM Bz.

Based on the observed redox potential values, CCET-based stability, and high solubility, H-cell charge/discharge cycling experiments were conducted to evaluate the practical stability of 1,2-dicarbonyl

compounds as potential anolytes for redox flow battery (RFB). Solvent and electrolyte effects were optimized using CV and cycling studies with benzil (Bz) as the model compound. Compared to weakly coordinating TBA^+-based electrolytes, Li^+ and K^+ were expected to better stabilize radical anions via stronger ion-pairing. While this ion-pairing effect has previously enhanced anolyte stability in NARFBs,[55] no cathodic shift in redox potential was observed for Bz in 0.5 M LiTFSI in DMF (Fig. 5a, S1). Moreover, $TBAPF_6$ enabled the longest cycling lifetime, whereas LiTFSI and KPF_6 showed capacity fade before 100 cycles (Fig. 5a). To investigate this unexpected trend, DFT calculations were performed for Bz radical anions paired with Li^+ and K^+. Both cations coordinated in a bridged fashion, favoring *cis*-conformations (dihedral angles: 10.8° for Li^+, 12.7° for K^+) that are less stable than the *trans*-planar form (Fig. 5b). These results suggest that despite stronger coordination, Li^+ and K^+ destabilize Bz radical anions by enforcing less favorable geometries—further highlighting the role of weakly coordinating $TBAPF_6$ in promoting CCET-driven stability.

Lastly, static H-cell cycling in 0.5 M $TBAPF_6$/DMF confirmed this trend, and results are summarized in Fig. 5c. Despite having a more negative redox potential, Bz retained 100% of its capacity over 100 cycles, outperforming PQ (75% fade, 100 cycles) and ANQ (15% fade, 60 cycles). Similar trends were observed in thiophene-based 1,2-dicarbonyls: 2,2'-thenil showed 0% fade over 390 cycles, surpassing 2,2'-BDTP (10% fade, 280 cycles), 3,3'-thenil (14% fade, 300 cycles), and 4,4'-BDTP (75% fade, 60 cycles). Although furil exhibited capacity fade after 125 cycles, it still outperformed PQ, ANQ, and 4,4'-BDTP (Fig. S20). Moreover, post-cycling CV analyses showed minimal degradation for Bz, in contrast to significant signal loss for PQ (Fig. 5d). Overall, these results break the conventional scaling relationship that links greater radical anion stability to milder redox potentials. Instead, CCET emerges as a key stabilization mechanism, enabling access to more reducing potentials without compromising cycling performance, a valuable strategy for the development of next-generation ROMs in energy storage.

Conclusion

We demonstrate a reversible and stable CCET mechanism using simple acyclic 1,2-dicarbonyl compounds as model system. Through electrochemical, spectroscopic, and computational analyses, we reveal the presence of conformational change upon electron transfer and its influence on radical anion stability. By comparing acyclic Bz and cyclic PQ, CCET was shown to stabilize the Bz radical anion by forming the *trans*-planar geometry, which minimizes electron repulsion and enables greater delocalization. Whereas greater stability is often associated with less extreme redox potentials, the presented results demonstrate a stabilization mechanism that achieves high stability while accessing more negative redox potentials, which is especially attractive for energy storage applications. Under charge/discharge cycling conditions, the flexible acyclic 1,2-dicarbonyl compounds demonstrated robust stability (over their rigid cyclic analogs), enabling the identification of these class of ROMs as simple and low-cost anolytes for potential RFB applications. On going research in our laboratory is focused on further exploring the practical application of these compounds in electrocatalysis and energy systems.

Data Availability All experimental data, computational data, and copies of spectra are available in the supplementary information.

Competing interests Northwestern University has filed a provisional patent that describes the development of reversible electron transfer coupled with geometric isomerization in 1,2-dicarbonyl compounds and their application to energy and catalysis on behalf of the inventors A.K., J.M.E., and C.A.M. The remaining authors declare no competing interests.

Acknowledgements This work was supported by Northwestern University with a start-up grant for C.A.M. and a seed grant from the Paula M. Trienens Institute for Sustainability and Energy at Northwestern University (Decarbonization Store Pillar). The facilities at IMSERC at Northwestern University were used with funding support from the Soft and Hybrid Nanotechnology Experimental (SHyNE) Resource (NSF ECCS-2025633), International Institute of Nanotechnology, and Northwestern University. This research was supported in part through the computational resources and staff contributions provided for the Quest high performance computing facility at Northwestern University which is jointly supported by the Office of the Provost, the Office for

Research, and Northwestern University Information Technology. A.K. was supported by the Quad Fellowship, Institute of International Education. We thank K. Tsay, M. Judd, R. Chaklashiya, and S. Han at Northwestern University for assistance with EPR measurements and simulations and Selim Alayoglu at the Reactor Engineering and Catalysis Testing at Northwestern University for assistance with IR and Raman analysis.

Author Contributions A.K., J.M.E., and C.A.M. conceived the work and designed the experiments. A.K. performed the synthesis, electrochemical experiments, computational, and cycling studies. J.M.E. performed the FTIR and Raman spectroscopy studies. A.K., J.M.E., and C.A.M. wrote the manuscript and provided revisions. All authors have given approval to the final version of the manuscript. Correspondence should be addressed to christian.malapit@northwestern.edu

References

1. Banerjee, T. & Kundu, R. Mini-review on organic electrode materials: Recent breakthroughs and advancement in metal ion batteries. *Energy & Fuels* **38**, 12487–12509 (2024).
2. Hari Prasad, P. M., Malavika, G., Pillai, A., Sadan, S. & Pillai, Z. S. Emerging organic electrode materials for sustainable batteries. *NPG Asia Materials* **16**, 37 (2024).
3. Shaw, M. H., Twilton, J. & MacMillan, D. W. C. Photoredox catalysis in organic chemistry. *J. Org. Chem.* **81**, 6898–6926 (2016).
4. Torres-Méndez, C., Axelsson, M. & Tian, H. Small organic molecular electrocatalysts for fuels production. *Angew. Chem. Int. Ed.* **63**, e202312879 (2024).
5. Medici, F., Chiroli, V., Raimondi, L. & Benaglia, M. Latest updates in electrophotochemical reactions. *Tetrahedron Chem* **9**, 100061 (2024).
6. Liu, J., Lu, L., Wood, D. & Lin, S. New redox strategies in organic synthesis by means of electrochemistry and photochemistry. *ACS Cent. Sci.* **6**, 1317–1340 (2020).
7. Chai, J., Lashgari, A. & Jiang, J. Electroactive materials for next-generation redox flow batteries: from inorganic to organic. In *ACS Symposium Series* (eds. Qin, L. & Fan, L.-S.) vol. 1364 1–47 (American Chemical Society, Washington, DC, 2020).
8. Zhong, F., Yang, M., Ding, M. & Jia, C. Organic electroactive molecule-based electrolytes for redox flow batteries: status and challenges of molecular design. *Front. Chem.* **8**, 451 (2020).
9. Kowalski, J. A., Su, L., Milshtein, J. D. & Brushett, F. R. Recent advances in molecular engineering of redox active organic molecules for nonaqueous flow batteries. *Curr. Opin. Chem. Eng.* **13**, 45–52 (2016).
10. Li, M. *et al.* Experimental protocols for studying organic non-aqueous redox flow batteries. *ACS Energy Lett.* **6**, 3932–3943 (2021).
11. Elgrishi, N. *et al.* A practical beginner's guide to cyclic voltammetry. *J. Chem. Educ.* **95**, 197–206 (2018).
12. Murray, P. R. D. *et al.* Photochemical and electrochemical applications of proton-coupled electron transfer in organic synthesis. *Chem. Rev.* **122**, 2017–2291 (2022).
13. Gentry, E. C. & Knowles, R. R. Synthetic applications of proton-coupled electron transfer. *Acc. Chem. Res.* **49**, 1546–1556 (2016).
14. Tyburski, R., Liu, T., Glover, S. D. & Hammarström, L. Proton-coupled electron transfer guidelines, fair and square. *J. Am. Chem. Soc.* **143**, 560–576 (2021).
15. Shi, R. R. S., Tessensohn, M. E., Lauw, S. J. L., Foo, N. A. B. Y. & Webster, R. D. Tuning the reduction potential of quinones by controlling the effects of hydrogen bonding, protonation and proton-coupled electron transfer reactions. *Chem. Commun.* **55**, 2277–2280 (2019).
16. Mayer, J. M. Proton-coupled electron transfer: A reaction chemist's view. *Annual Review of Physical Chemistry* vol. 55 363–390 (2004).
17. Cannon, C. G., Klusener, P. A. A., Brandon, N. P. & Kucernak, A. R. J. Aqueous redox flow batteries: small organic molecules for the positive electrolyte species. *ChemSusChem* **16**, e202300303 (2023).
18. Feng, R. *et al.* Reversible ketone hydrogenation and dehydrogenation for aqueous organic redox flow batteries. *Science* **372**, 836–840 (2021).
19. Corrado, F. *et al.* Azobenzene-based optoelectronic transistors for neurohybrid building blocks. *Nat. Commun.* **14**, 6760 (2023).
20. Bandara, H. M. D. & Burdette, S. C. Photoisomerization in different classes of azobenzene. *Chem. Soc. Rev.* **41**, 1809–1825 (2012).
21. Schatz, D. & Wegner, H. A. Electrochemistry of azobenzenes and its potential for energy storage. *J. Org. Chem.* **90**, 5336–5342 (2025).

22. Zhang, L. *et al.* Reversible redox chemistry in azobenzene-based organic molecules for high-capacity and long-life nonaqueous redox flow batteries. *Nat. Commun.* **11**, 3843 (2020).
23. Pombeiro, A. J. L., Silva, M. F. C. G. da & Lemos, M. A. N. D. A. Electron-transfer induced isomerizations of coordination compounds. *Coord. Chem. Rev.* **219–221**, 53–80 (2001).
24. Liu, Y. *et al.* Effective design strategy of small bipolar molecules through fused conjugation toward 2.5 V based redox flow batteries. *ACS Energy Lett.* **7**, 1274–1283 (2022).
25. Hasan, F., Mahanta, V. & Abdelazeez, A. A. A. Quinones for aqueous organic redox flow battery: A prospective on redox potential, solubility, and stability. *Adv. Mat. Interfaces* **10**, 2300268 (2023).
26. Symons, P. Quinones for redox flow batteries. *Curr. Opin. Electrochem.* **29**, 100759 (2021).
27. Huang, S. *et al.* Molecular engineering of dihydroxyanthraquinone-based electrolytes for high-capacity aqueous organic redox flow batteries. *Nat. Commun.* **13**, 4746 (2022).
28. Talvitie, J. *et al.* Electron-deficient phenanthrenequinone derivative for photoactivated hydrogen atom transfer mediated oxidation of secondary alcohols. *ChemPhotoChem* **7**, e202300107 (2023).
29. Ding, Y., Li, Y. & Yu, G. Exploring bio-inspired quinone-based organic redox flow batteries: A combined experimental and computational study. *Chem* **1**, 790–801 (2016).
30. Ebihara, K., Hiura, H. & Takahashi, H. Time-resolved resonance Raman studies of the structures of the lowest triplet state and the radical anion of benzil. *J. Phys. Chem.* **96**, 9120–9127 (1992).
31. Dominguez, M. *et al.* Electrochemical reduction of benzil in strongly acid and alkaline media. *J. Electroanal Chem. Interfacial Electrochem.* **316**, 133–142 (1991).
32. Vincenz-Chodkowska, A. & Grabowski, Z. R. Change of reactivity of polarizable molecules in the electric field of the double layer—II. Cis-trans isomerization of stilbenediol. *Electrochim. Acta* **9**, 789–801 (1964).
33. Juchnovski, I. N. & Kolev, Ts. M. Infrared spectra and configuration of anion radical and dianion of benzil and benzil-^{18}O. *Spectrosc. Lett.* **19**, 529–543 (1986).
34. Yasui, M. *et al.* Synthesis and luminescence properties of substituted benzils. *Commun. Chem.* **6**, 245 (2023).
35. Brown, C. J. & Sadanaga, R. The crystal structure of benzil. *Acta Crystallogr.* **18**, 158–164 (1965).
36. Pawelka, Z., Koll, A. & Zeegers-Huyskens, T. Solvent effect on the conformation of benzil. *J. Mol. Struct.* **597**, 57–66 (2001).
37. Kanagathara, N., Senthilkumar, K., Sabari, V., Ragavendran, V. & Elangovan, S. Structural and vibrational investigation of benzil-(1,2-diphenylethane-1,2-dione): experimental and rheoretical studies. *J. Chem.* **2022**, 5968496 (2022).
38. Yoo, D.-J., Heeney, M., Glöcklhofer, F. & Choi, J. W. Tetradiketone macrocycle for divalent aluminium ion batteries. *Nat. Commun.* **12**, 2386 (2021).
39. Meng, J. *et al.* Cyclotetrabenzil derivatives for electrochemical lithium-ion storage. *Angew. Chem. Int. Ed.* **62**, e202300892 (2023).
40. Jarvid, M. *et al.* Tailored side-chain architecture of benzil voltage stabilizers for enhanced dielectric strength of cross-linked polyethylene. *J. Polym. Sci. Part B: Polym. Phys.* **52**, 1047–1054 (2014).
41. Park, S. Y. *et al.* Nanoparticulate conjugated microporous polymer with post-modified benzils for enhanced pseudocapacitor performance. *Chem. Eur. J.* **26**, 12343–12348 (2020).
42. Cong, C., Kim, J., Gannett, C. N., Abruña, H. D. & Milner, P. J. Unexpected direct synthesis of tunable redox-active benzil-linked polymers via the benzoin reaction. *ACS Appl. Polym. Mater.* **5**, 1056–1066 (2023).
43. Singh, A. K., Palit, D. K. & Mittal, J. P. Conformational relaxation dynamics in the excited electronic states of benzil in solution. *Chem. Phys. Lett.* **360**, 443–452 (2002).
44. Solin, S. A. & Ramdas, A. K. Raman spectrum of crystalline benzil. *Phys. Rev.* **174**, 1069–1075 (1968).
45. Mizuno, M., Iwata, K. & Takahashi, H. Time-resolved infrared and resonance Raman studies of benzil. Vibrational analysis and structures of the excited states. *J. Mol. Struct.* **661–662**, 3–10 (2003).
46. Hanuza, J. *et al.* Spontaneous and stimulated Raman scattering and infrared spectra of benzil ($C_{14}H_{10}O_2$) crystal: promoting modes of the stimulated effect, anharmonicity and scaling factors of fundamental vibrations. *J. Raman Spectrosc.* **35**, 224–235 (2004).
47. Cumper, C. W. N. & Thurston, A. P. Electric dipole moments and molecular conformations of benzophenones, benzils, benzhydrols, and benzoins. *J. Chem. Soc., Perkin Trans. 2* 106–111 (1972) doi:10.1039/P29720000106.
48. Das, K. K. & Majumdar, D. Ground and excited states of benzil: A theoretical study. *J. Mol. Struct: THEOCHEM* **288**, 55–61 (1993).

49. Kolev, T. M. & Stamboliyska, B. A. Vibrational spectra and structure of benzil and its 18O- and d10-labelled derivatives: a quantum chemical and experimental study. *Spectrochimica Acta Part A: Molecular and Biomolecular Spectroscopy* **58**, 3127–3137 (2002).
50. Ebihara, K., Hiura, H. & Takahashi, H. Time-resolved resonance Raman studies of the structures of the lowest triplet state and the radical anion of benzil. *J. Phys. Chem.* **96**, 9120–9127 (1992).
51. Hanuza, J. *et al.* Spontaneous and stimulated Raman scattering and infrared spectra of benzil (C_{14} H_{10} O_2) crystal: promoting modes of the stimulated effect, anharmonicity and scaling factors of fundamental vibrations. *J Raman Spectrosc.* **35**, 224–235 (2004).
52. Mizuno, M., Iwata, K. & Takahashi, H. Time-resolved infrared and resonance Raman studies of benzil. Vibrational analysis and structures of the excited states. *J. Mol. Struct.* **661–662**, 3–10 (2003).
53. Hwang, S. *et al.* Integration of Functional Groups to Enhance the Solubility and Stability of Viologen in Aqueous Organic Redox Flow Batteries. *ACS Appl. Mater. Interfaces* **16**, 28645–28654 (2024).
54. Singh, V. *et al.* Controlling π–π interactions of highly soluble naphthalene diimide derivatives for neutral pH aqueous redox flow batteries. *Adv. Mater.* **35**, 2210859 (2023).
55. Ahn, S. *et al.* Stabilization of naphthalene diimide anions by ion pair formation in nonaqueous organic redox flow batteries. *J. Am. Chem. Soc.* **146**, 4521–4531 (2024).

Supplementary Files

This is a list of supplementary files associated with this preprint. Click to download.

- CCETSI.pdf